International Journal of Nanomedicine

Dovepress
open access to scientific and medical research

Open Access Full Text Article

ORIGINAL RESEARCH

Flower-shaped ZnO nanoparticles synthesized by a novel approach at near-room temperatures with antibacterial and antifungal properties

This article was published in the following Dove Press journal:
International Journal of Nanomedicine
10 February 2014
Number of times this article has been viewed

Mohd Farhan Khan[1,2]
M Hameedullah[1]
Akhter H Ansari[1]
Ejaz Ahmad[3]
MB Lohani[2]
Rizwan Hasan Khan[3]
M Mezbaul Alam[4]
Wasi Khan[5]
Fohad Mabood Husain[6]
Iqbal Ahmad[6]

[1]NanoSolver Lab, Department of Mechanical Engineering, Zakir Hussain College of Engineering and Technology, Aligarh Muslim University, Aligarh, India; [2]Department of Applied Chemistry, Integral University, Lucknow, India; [3]Interdisciplinary Biotechnology Unit, Aligarh Muslim University, Aligarh, India; [4]Chemistry Department, College of Science, King Saud University, Riyadh, Kingdom of Saudi Arabia; [5]Centre of Excellence in Materials Science (Nanomaterials), Department of Applied Physics, Zakir Hussain College of Engineering and Technology, Aligarh Muslim University Aligarh, India; [6]Department of Agricultural Microbiology, Faculty of Agricultural Sciences, Aligarh Muslim University, Aligarh, India

Correspondence: Mohd Farhan Khan
NanoSolver Lab, Department of Mechanical Engineering, Zakir Hussain College of Engineering and Technology, Aligarh Muslim University, Aligarh 202002, India
Tel +91 955 763 6109
Email mfk.iitkgp@gmail.com

Rizwan Hasan Khan
Interdisciplinary Biotechnology Unit, Aligarh Muslim University, Aligarh 202002, India
Email rizwanhkhan@hotmail.com

Abstract: Due to enormous applications of metal oxide nanoparticles in research and health-related applications, metal oxide nanoparticles are increasingly being developed through cheaper and more user-friendly approaches. We have formulated a simple route to synthesize zinc oxide nanoparticles (ZNPs) by a sol–gel method at near-room temperatures 25°C, 35°C, 55°C, and 75°C. The results are analyzed by X-ray diffraction, scanning electron microscopy with energy-dispersive X-ray spectroscopy, and ultraviolet-visible absorption spectroscopy. The effect of different temperature conditions (25°C–75°C) on the particulate sizes (23.7–88.8 nm), pH levels (11.7–11.9), and morphologies (slender needle–broad arrow) of flower-shaped ZNP colonies is studied. A possible mechanism depicting the growth rates at different temperatures and of different facets, mainly towards the <0 0 0 1> and <0 1 $\bar{1}$ 0> planes of the ZNPs has also been discussed. The values of λ_{max} (293–298 nm) suggest that ZNPs prepared at 55°C are the most effective ultraviolet B absorbers, and that they can be used in sunscreens. Highly significant antimicrobial activity against medically important Gram-positive (*Staphylococcus aureus*) and Gram-negative (*Escherichia coli*) bacteria and fungi (*Candida albicans*) by these ZNPs was also revealed. As *S. aureus* and *C. albicans* are responsible for many contagious dermal infections such as abscesses, furuncles, carbuncles, cellulitis, and candidiasis, we can postulate that our fabricated ZNPs may be useful as antimicrobial agents in antiseptic creams and lotions for the treatment of skin diseases.

Keywords: antimicrobial activity, cetyl trimethyl ammonium bromide, flower-shape zinc oxide nanoparticles, near-room temperature, sol–gel method, skin disease

Introduction

Zinc oxide (ZnO) is an n-type semiconductor that has a wide band gap of approximately 3.3 eV, along with a large excitation binding energy of 60 meV (at 298 K).[1,2] ZnO has the good property of being able to produce blue-green luminescence and absorption in the ultraviolet (UV) region, which is exploited for sunscreens, textile industries, catalysts, sensors, photodetectors, and for obtaining solar energy.[3–10] Keeping the scope of its applications in mind, the different morphologies of ZnO nanoparticles (ZNPs) are developed as nanoflowers, nanorods, nanowhiskers, nanobelts, nanotubes, nanorings, nanocolumns, and so on.[11–17]

Different methods that are used for the production of ZNPs include the sol–gel method, facile hydrothermal method, solution method, electric current heating method; solvothermal method, self-propagating high-temperature synthesis method, spontaneous nucleation method, spray pyrolysis, gas-phase reaction method, laser ablation method, thermal evaporation, and so on.[18–31] The different parameters that are generally used require temperatures ranging from low to more than 1,500°C, pressures from 1 atm to a

few mTorr, and various other reaction conditions, leading to the development of complicated and costly systems. So, there is a challenge in developing cheaper and more user-friendly systems for the production of ZNPs. In this regard, several reports are available that are neither feasible nor cost effective. The hydrothermal preparation of flower-like ZnO nanorods is maintained at more than 120°C, for several hours, at a pH of 13.5;[32] chrysanthemum-like ZnO nanorods are maintained in the presence of sodium dodecyl sulfate at 120°C for 24 hours[33] and 10 hours,[34,35] and the preparation of flower-like ZnO microstructures was conducted via sonochemical treatment for 1 hour.[36] These are a few examples of complicated syntheses. In short, the synthesis of ZNPs at near-room temperature was required, while considering crystallite size, pH levels, and morphology in order to avoid costly and complicated systems that are utilized for various low-temperature UV-captivating medications and devices. A previously reported approach used to synthesize ZNPs by our group involves low temperatures, below the boiling point of water, while avoiding sophisticated equipment.[37]

In this work, the simple sol–gel synthesis of flower-shaped ZNPs, at near-room temperatures (at 25°C, 35°C, 55°C, and 75°C), employing zinc acetate diyhdrate (ZAD), NaOH in the presence of the cationic surfactant, and cetyl trimethyl ammonium bromide (CTAB), has been reported. Along with the different techniques that have been used for the characterization of synthesized flower-shaped ZNPs – like X-ray diffraction (XRD), scanning electron microscopy (SEM) with energy-dispersive X-ray spectroscopy (EDS) and UV-visible (UV-vis) spectroscopy – the effect of different temperature conditions on the crystallite size, pH, and morphology of the flower-shaped ZNPs, as well as a simple growth mechanism, have been discussed. Finally, the antimicrobial activity of synthesized ZNPs was tested against both Gram-positive and Gram-negative bacteria and fungi.

Materials and methods

Materials

All of the chemicals (ie, $Zn[Ac]_2 \cdot 2H_2O$ or ZAD and NaOH) were procured from Merck KGaA (Darmstadt, Germany). The capping agent, CTAB, was purchased from LobaChemie Pvt Ltd (Mumbai, India). These agents all were used as received without further purification. The glassware was purchased from Borosil® Glass Works Limited (Mumbai, India), and double-distilled water was used throughout the synthesis.

Synthesis of ZNPs

In a simple preparation, 0.2 g of CTAB was added to bi-distilled (BD) water, in a flat-bottomed flask. The system was kept on magnetic stirring along with heating. Subsequently, 5% (ie, 21.94 g) ZAD of a 100 mL solution was added to the reaction mixture. Under steady stirring conditions, the NaOH solution was added drop-wise to the flask. After few minutes of stirring, the colloidal solution took on a milky appearance. The setup was cooled, centrifuged, dried at room temperature, and washed with BD water and methanol for the ZNP characterization (Figure 1). The whole synthesis was carried out without any unusual treatment. Finally, the samples of ZNPs were stored for further characterization.

Characterization of ZNPs

X-ray diffraction (XRD)

The crystallinity and phases of the ZNPs were characterized by an X-ray diffractometer (D8 ADVANCE; Bruker AXS Inc, Madison, WI, USA) using a monochromatized X-ray beam with nickel-filtered Cu-K_α radiation in the 2θ range of 30°–70° with a step size of 0.01° and a scanning rate of 0.02 steps/second. The X-rays used for this purposed were generated at 40 kV and 40 kA.[38] The ZNPs crystallite size (D) was calculated from the highest intense peak (101) using the Debye–Scherrer equation:

$$D = \frac{k\lambda}{\beta \cos\theta}, \quad [1]$$

where k is the proportionality constant or shape factor and its value is 0.9; λ is the X-ray wavelength coming from Cu-K_α, and its value is 1.54178 Å; β is the full width at half maxima of the diffraction peak in radians; θ is the Braggs' angle in degrees.[39] The calculation was simplified by the inbuilt software, DIFFRACplus (Bruker AXS Inc).

Scanning electron microscopy (SEM) with energy-dispersive X-ray spectroscopy (EDS)

The morphology of ZNPs were carried out using SEM (JSM-6510 LV; JEOL, Tokyo, Japan), with an Oxford EDS System attachment (Oxford Instruments plc, Abingdon, UK). To avoid charging the mechanism during SEM measurement, the powder samples were coated by gold sputtering.[40,41]

UV-visible spectrophotometer

With the help of a double-beam PerkinElmer UV-vis spectrophotometer (PerkinElmer, Waltham, MA, USA), the absorbance spectra of ZNPs were measured in the quartz cuvette with a 1 cm path length. The BD water was used as a reference material for background correction.[42]

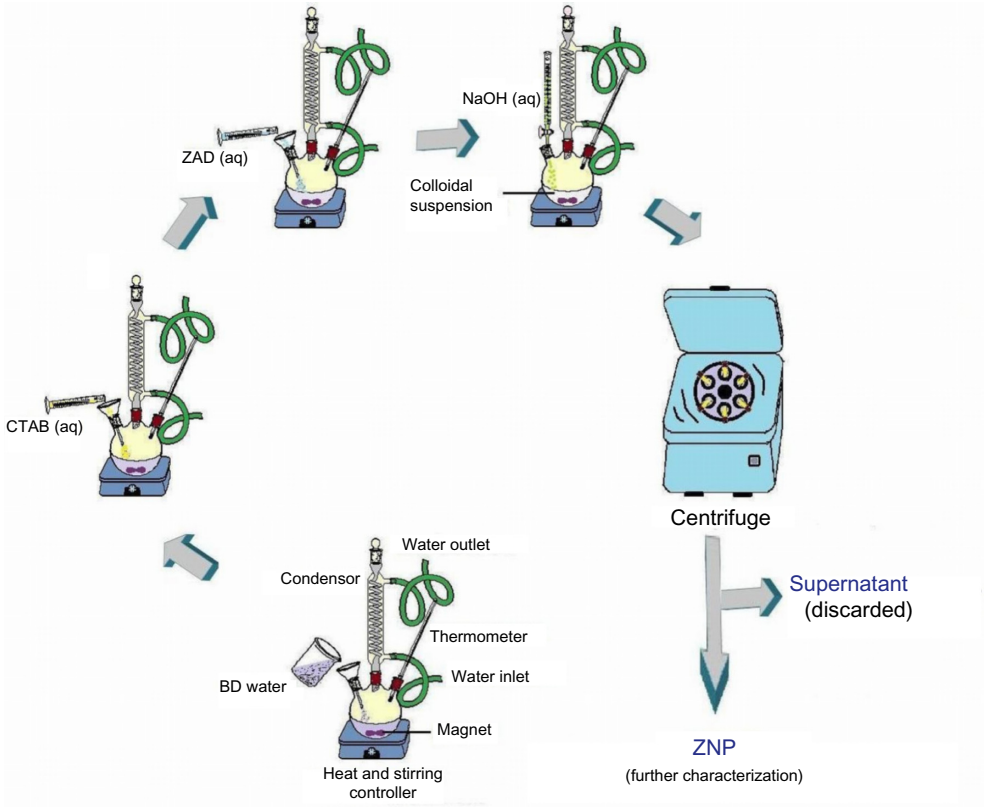

Figure 1 Flow diagram for the synthesis of ZNPs at different temperatures.
Abbreviations: ZAD, zinc acetate dihydrate; aq, aqueous; CTAB, cetyl trimethyl ammonium bromide; BD, bi-distilled; ZNPs, zinc oxide nanoparticles.

Determination of antibacterial and antifungal activity of ZNPs

The ZNPs synthesized at near-room temperatures (25°C, 35°C, 55°C, and 75°C) were tested for bactericidal as well as fungicidal activity via the disc-diffusion method against both Gram-positive (*Staphylococcus aureus*) and Gram-negative (*Escherichia coli*) bacteria, as well as fungi (*Candida albicans*). The antibacterial activity of ZNPs was performed using the filter paper disc method.[43] All cultures were routinely maintained on nutrient agar (NA) and incubated at 37°C overnight. The culture was centrifuged at 1,000 rpm, and pellets were resuspended and diluted in sterile normal saline solution to obtain the viable count of 10^5 cfu/mL. Diluted bacterial culture suspension (0.1 mL) was spread uniformly, with the help of a spreader, on NA plates. Sterile 8 mm discs (HiMedia Laboratories Pvt Ltd, Mumbai, India) were impregnated with the ZNPs. The plates were then incubated at 37°C for 24 hours. The antifungal activity of ZNPs were also performed using the same methods described previously, but with slight differences. All cultures were routinely maintained on sabouraud dextrose agar (SDA) and incubated at 28°C. Further, the inoculums of non-sporing fungi, *C. albicians* were performed by growing the culture in Sabouraud dextrose broth at 37°C overnight. A total of 0.1 mL of diluted fungal culture suspension was spread uniformly, with the help of a spreader, on SDA plates. *C. albicans* plates were incubated at 37°C for 18–48 hours. An antibiotic disc (0.03 mg/disc; HiMedia Laboratories Pvt Ltd), doxycycline (for bacteria), and nystatin (for fungi) were used as standard. Media with ZnO powder of same concentration was set up as the control. The diameters of the resulting inhibition zones (in mm) of microbial growth were measured for the determination of antibacterial and antifungal activities.[44]

Results and discussion

X-ray diffraction analysis

X-ray diffractograms were analyzed to obtain information about various crystalline aspects of ZNPs. The sharp and intense peaks shown in Figure 2 indicated that the sample ZNPs were highly crystalline, with polycrystalline structures. The XRD patterns showed broad peaks at 2θ of 31°, 34°, 36°, 57°, 67°, and 69°, corresponding to the diffraction planes of 100, 002, 101, 110, 112, and 201 of ZnO crystals, respectively. Therefore, almost all the samples, which formed at different temperatures, exhibited similar peak patterns (Figure 2). The XRD pattern of the different samples of ZNPs formed

at 25°C, 35°C, 55°C, and 75°C were in accordance with the standard peaks displayed by the International Centre for Diffraction Data, and they proved to be characteristic structures of hexagonal wurtzite, with the lattice constant (c/a) of 1.6 where *a* and *c* are 3.24 Å and 5.20 Å, respectively. In addition, the peaks (100), (002), and (101) clearly indicate formation of pure wurtzite structure of ZnO.[45] Therefore, the XRD pattern showed that samples were formed in single phase. The high intensity of (100) peak at 31° suggested the growth of ZNPs along the easy direction of crystallization.[46] No other peaks related to impurities were detected in the XRD spectra, confirming the pure form of the synthesized ZNPs. By applying the Debye–Scherrer equation to the full width at half maxima of the 100 diffraction plane, the average crystallite size of temperature-induced ZNPs at 25°C, 35°C, 55°C, and 75°C were found to be 23.7 nm, 82.5 nm, 69.6 nm, and 88.8 nm, respectively (Table 1). Therefore, the peak widths are inversely related to the crystallite sizes.

Scanning electron microscopy (SEM) and energy-dispersive X-ray spectroscopy (EDS)

The morphology of ZNPs was studied with the help of SEM. The morphological observations of the ZNPs formed at various temperature conditions (25°C, 35°C, 55°C, and 75°C) were accomplished with the help of four different

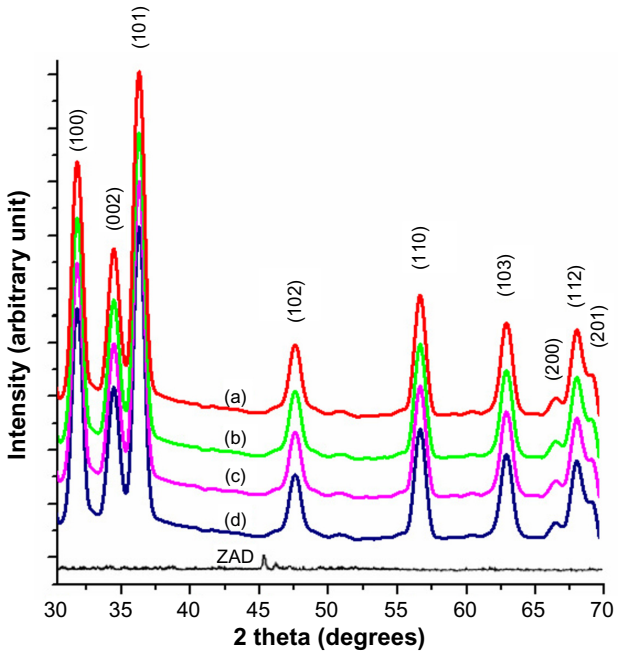

Figure 2 XRD of ZNPs prepared at different temperature conditions.
Notes: The following temperatures were used: (**a**) 25°C; (**b**) 35°C; (**c**) 55°C; and (**d**) 75°C.
Abbreviations: XRD, X-ray diffraction; ZNPs, zinc oxide nanoparticles; ZAD, zinc acetate dihydrate.

Table 1 The effect of various reaction conditions at near-room temperature (ie, 25°C, 35°C, 55°C, and 75°C) on the synthesis and characteristics of flower-shaped ZNPs

Sample	Crystallite size (nm)	Maximum absorbance (nm)	Final pH
ZNPs (25°C)	23.7	298	11.9
ZNPs (35°C)	82.5	295	11.7
ZNPs (55°C)	69.6	293	11.8
ZNPs (75°C)	88.8	294	11.9

Abbreviation: ZNPs, zinc oxide nanoparticles.

samples. The SEM results of these samples are shown in Figure 3A–D. All of the figures show the distinctive and abundant flower-shaped ZNPs, which were principally the ZNPs whose concentrations depict the variations at different temperatures, as shown in Table 1. The observations illustrate that there are huge hexagonal arrays of ZNPs assimilated to form flower-shaped bundles (Table 1). Here, the SEM patterns agree well with the XRD results in terms of both size and shape.

The composition analysis of the flower-shaped ZNPs from the EDS plot of the SEM images are shown in Figure 4A–D, which was meant for the samples prepared at the temperature conditions of 25°C, 35°C, 55°C, and 75°C. The EDS readings proved that the required phase of Zn and O are present in the samples. Along with the Zn and O phases, some additional peaks are apparent, which is probably due to the presence of substrate, over which the nanoparticle samples were held during SEM imaging.

UV-visible absorption spectroscopy

The optical study of the flower-shaped ZNPs was performed with the help of a double-beam UV-vis spectrophotometer at room temperature; the results are shown in Figure 5 for ZNPs synthesized at all of the different temperature conditions. The present results were reported after few minutes of sample preparation; the results are in agreement with those of Guan et al.[47] The peaks of all different spectra recorded during different temperature conditions occurred in the UV-B region (ie, 280–320 nm), with differences noted in absorbance intensity as well as in wavelength maxima (λ_{max}). Our findings are in accordance with those from previously reported studies, proving that peak shifts depend upon the crystallite's size, the effect of the solvent, reaction temperature, synthesis method, and the aging of samples.[21,48] The spectrum of the solution of ZNPs prepared at 55°C showed maximum absorbance with the lowest λ_{max} at 293 nm, whereas the spectrum of the solution of ZNPs prepared at 25°C showed minimum absorbance with the highest λ_{max}

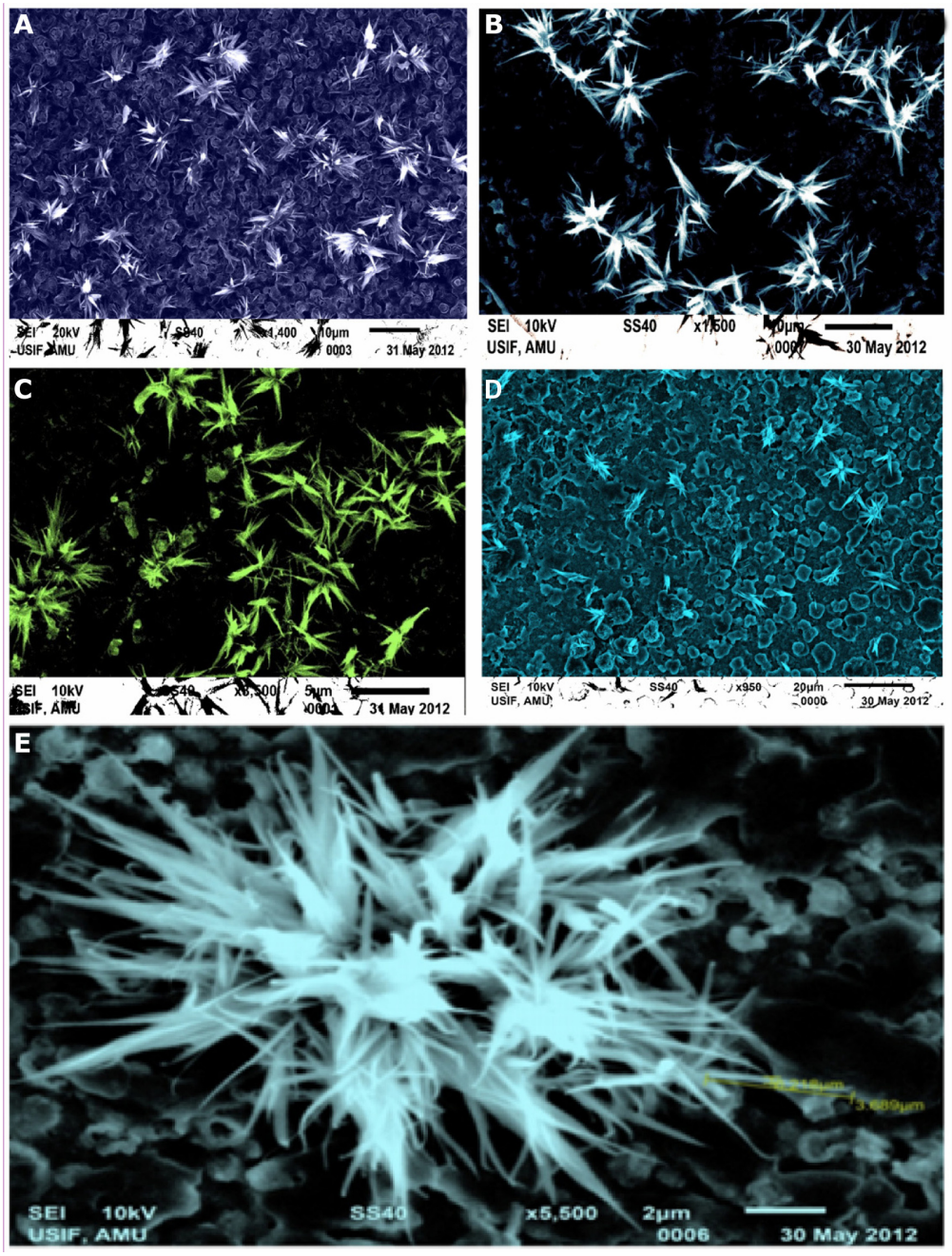

Figure 3 SEM photographs of flower-shaped ZNPs in different temperature conditions.
Notes: (**A**) 25°C; (**B**) 35°C; (**C**) 55°C; (**D**) 75°C; and (**E**) enlarged SEM photograph of flower-shaped ZNPs prepared at 35°C.
Abbreviations: SEM, scanning electron microscopy; ZNPs, zinc oxide nanoparticles.

at 298 nm (Table 1). UV-B light is mostly absorbed by the ozone layer, but due to continuous ozone depletion, a low amount of rays reach the Earth's surface causing sunburn, skin tanning, skin cancer, mutations, thymine dimerization, double-strand deoxyribonucleic acid breakage, vitamin A, damage and collagen damage. Therefore, the values of λ_{max} suggest that ZNPs prepared at 55°C are the most effective UV-B absorbers. Absence of other peaks in the spectrum confirms the purity of synthesized ZNPs.

Effect of temperature on the crystallite size of the ZNPs

By changing the reaction temperature conditions, the average crystallite sizes of flower-shaped ZNPs were reported. At 25°C, the ZNPs' crystallite size was 23.73 nm. Upon further increasing the synthesis temperature to 35°C, the crystallite size increased to 82.58 nm. However, at 55°C, the size showed a slight decrease to 69.65 nm. At 75°C, the ZNPs' crystallite size increased to 88.82 nm. A brief comparison

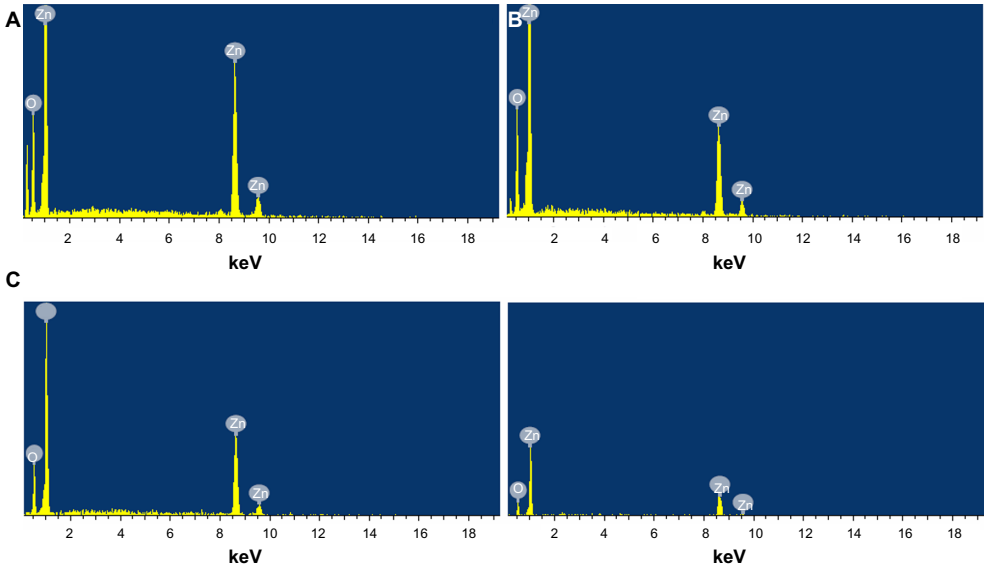

Figure 4 EDS of flower-shaped ZNPs prepared at different temperature conditions.
Notes: (**A**) 25°C; (**B**) 35°C; (**C**) 55°C; and (**D**) 75°C.
Abbreviations: EDS, energy-dispersive X-ray spectroscopy; ZNPs, zinc oxide nanoparticles.

of different crystallite sizes is presented in Table 1. Similarly, Li et al also fabricated the flower-like and cabbage-like ZnO micro- and nanostructures, but at temperatures of 120°C, 150°C, and 180°C.[35] In Figure 3E, the dimensions of the ZNPs petals took on a flower-like morphology of the ZnO microstructures, as was previously reported.[36]

Effect of temperature on pH of ZNPs

The initial pH of the reacting species, like ZAD, CTAB, and NaOH was found to be 6.6, 11.7, and 12.5, respectively. Following synthesis, the pH of the flower-shaped ZNP solutions formed at 25°C, 35°C, 55°C, and 75°C were 11.9, 11.7, 11.8, and 11.9, respectively. Here, we reported the fabrication

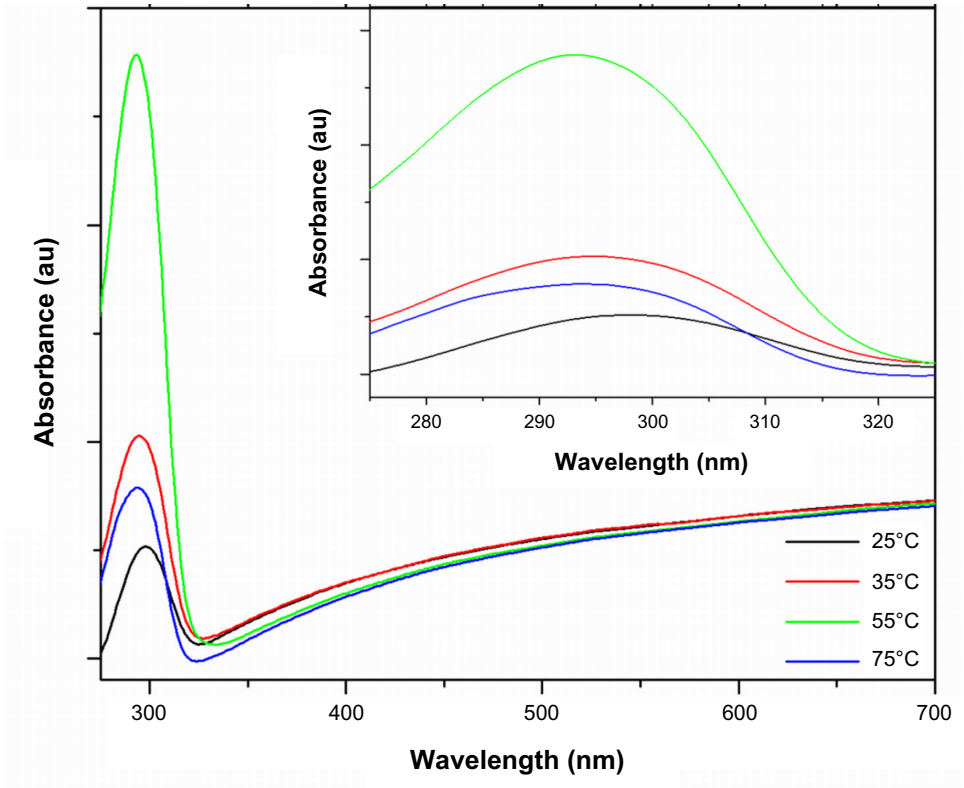

Figure 5 UV-vis spectra of flower-shaped ZNPs prepared in different temperature conditions.
Abbreviations: au, absorbance units; UV-vis, ultraviolet-visible spectroscopy; ZNPs, zinc oxide nanoparticles.

of flower-shaped ZNPs consisting of long and pointed rods at different near-room temperatures, as mentioned earlier. Zhang et al reported that flower-like ZnO nanostructures consisted of nanorods when the initial pH of NaOH was taken (13.5 at 120°C, 160°C, and 200°C).[49]

Effect of temperature on the morphology of ZNPs

The magnified morphology of the samples in different temperature conditions held a huge colony consisting of adequate bunches of flower-shaped ZNPs, which contained a large number of petals (Figure 3E). The petals are of two types: one with a broad diameter; and the other with a reduced cross-section. The broad arrow-like petals become smaller when the temperature is lowered. The slender needle-like petals are numerous, and their growth increases when the synthesis temperature is minimized. The density of these colonies increases while the size of these flowers decreases, which is based on moving down the temperature scale (ie, 75°C → 55°C → 35°C → 25°C). The density of the ZNP petals in each flower-shaped bunch are increased manifold upon fabricating the ZNPs at lower temperatures. The similar production of flower-like ZnO nanostructures was also reported by other groups, but with different techniques and extended heating times.[36]

Growth mechanism of flower-shaped ZNPs

The sol–gel method of ZNP preparation using ZAD, NaOH, and CTAB (the capping agent) resulted in a number of reversible reactions (Figure 6). As discussed in previous studies, the formation of $Zn(OH)_2$ leads to the development of $(Zn[OH]_4)^{2-}$ and ZnO. Due to the electrostatic force of attractions, the different types of developed complexes of CTAB and $(Zn[OH]_4)^{2-}$ adsorbed on the ZnO surfaces leads to the elongation of c-axis, which actively elongates towards the 000I facet.[32,50–52] This anisotropic growth leads to the formation of slender needle-like and broad arrow-like morphologies, thus giving rise to the bundles of flower-shaped ZNPs (Figure 3E).

During the complete process of synthesis, there are different possible combinations of ZAD with NaOH that occur in the presence of CTAB, facilitating a good alkaline environment. Initially, the pH of the reaction species achieved via CTAB and NaOH were measured as 11.7 and 12.5, respectively. As the synthesis advanced, in the alkaline atmosphere, the developing units in the process of crystal growth in ZNPs were $(Zn[OH]_4)^{2-}$. These were further disintegrated, and this led to the development of crystal growth configurations.

At low temperatures and in the presence of the alkaline CTAB and NaOH solution, the formation of active–inactive sites and the development of elongated ZNP arrays from $(Zn[OH]_4)^{2-}$ intermediates took place. In the course of the ZNPs' growth, the aggregation of $(Zn[OH]_4)^{2-}$ and CTAB occurred with the formation of active sites after nucleation. This growth is varied on different planes, mainly towards the <0 0 0 I> and <0 I $\bar{I}$ 0> facets. The growths of these two facets at different temperatures were studied in this work. In alkaline pH, the nucleation process led to further

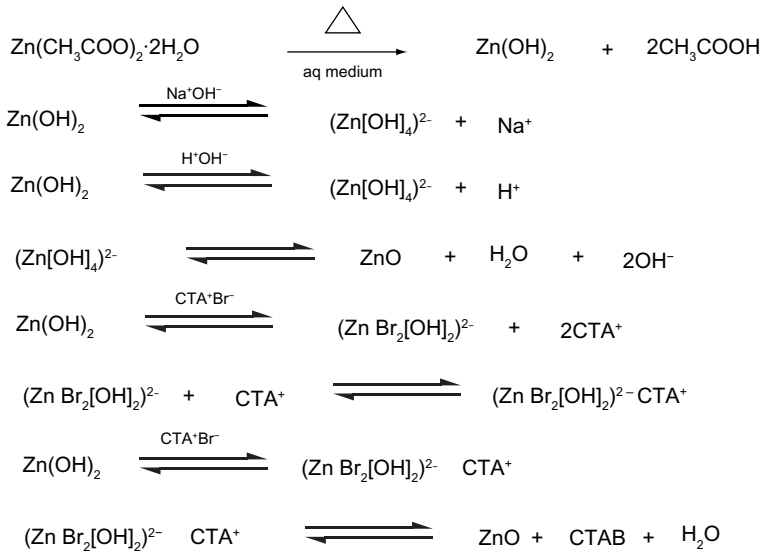

Figure 6 Reversible reactions involved in the sol–gel method of zinc oxide nanoparticle synthesis.
Abbreviation: aq, aqueous.

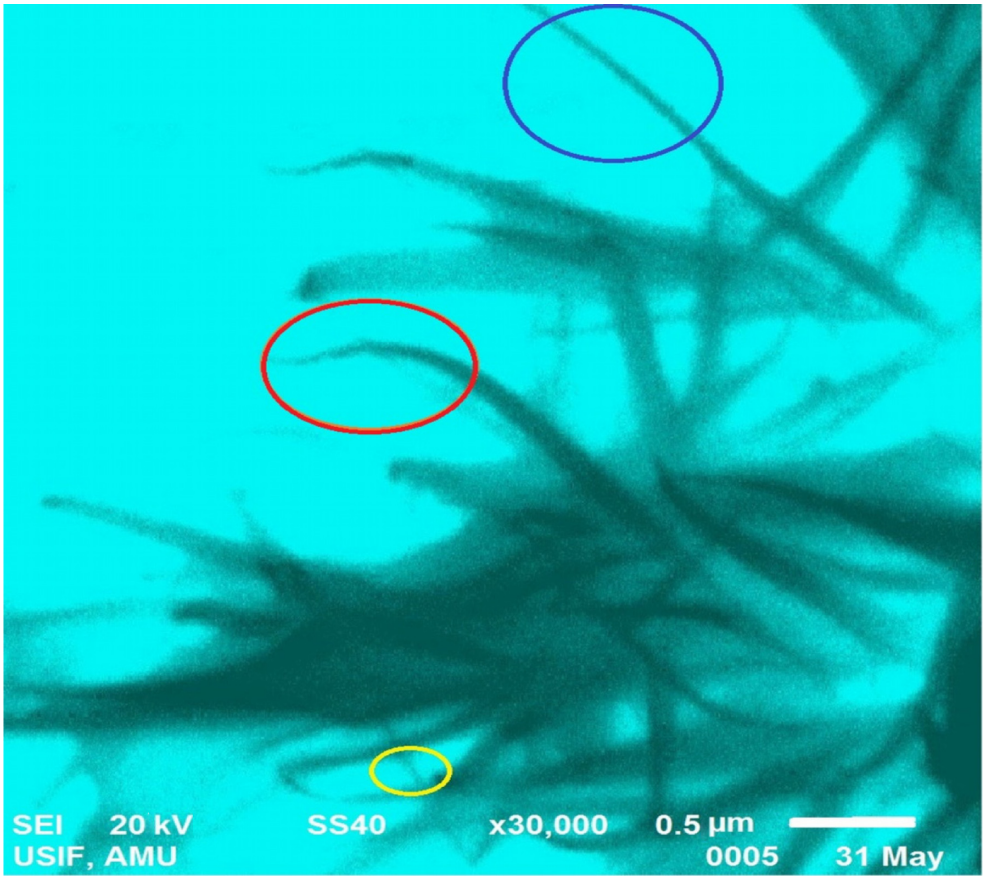

Figure 7 Growth order of the different morphologies of flower-shaped zinc oxide nanoparticle petals.
Notes: Slender needle-like morphology (encircled in blue and yellow), and broad arrow-like morphology (encircled in red).

unidirectional growth, generally as a function of the growth rate (gr), as follows:

$$\mathrm{gr}^{\langle 0\,0\,0\,1\rangle} > \mathrm{gr}^{\langle 0\,1\,\bar{1}\,1\rangle} > \mathrm{gr}^{\langle 0\,1\,\bar{1}\,0\rangle} > \mathrm{gr}^{\langle 0\,0\,0\,\bar{1}\rangle}. \quad [2]$$

Recent studies have shown that temperature has a minor effect on the morphology of ZNPs, but it does affect their size slightly.[52] At 25°C, the growth of slender needle-like ZNPs with a good aspect ratio increase in number from the broad arrow-like ZNPs, and this is due to the higher growth rate towards the <0 0 0 1> facets of the slender needle-like ZNPs. The overall growth rate of the slender needle-like ZNP sample at a pH of 11.9 (Figure 3A) is:

$$\mathrm{gr}^{\langle 0\,0\,0\,1\rangle} > \mathrm{gr}^{\langle 0\,1\,\bar{1}\,1\rangle} > \mathrm{gr}^{\langle 0\,1\,\bar{1}\,0\rangle}. \quad [3]$$

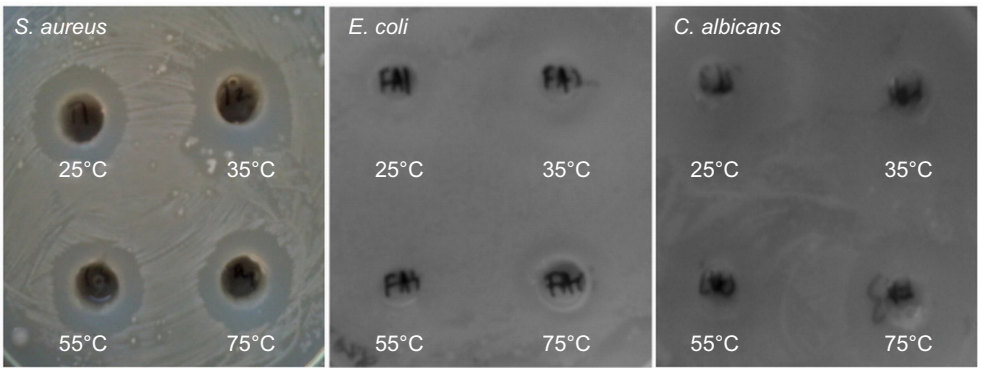

Figure 8 Antimicrobial activities of ZNPs prepared at different temperatures against Gram-positive (*S. aureus*) and Gram-negative (*E. coli*) bacteria, as well as fungi (*C. albicans*).
Abbreviations: *S. aureus*, *Staphylococcus aureus*; *E. coli*, *Escherichia coli*; *C. albicans*, *Candida albicans*; ZNPs, zinc oxide nanoparticles.

Table 2 Antimicrobial activity of ZNPs prepared at near-room temperatures

Sample	Concentration (mg/mL)	Zone of inhibition (mm)		
		Staphylococcus aureus (ATCC 25923)	*Escherichia coli* (ATCC 25922)	*Candida albicans*
ZNPs (25°C)	0.25	–	–	–
	0.50	20	21	14
ZNPs (35°C)	0.25	14	11	13
	0.50	21	18	19
ZNPs (55°C)	0.25	10	13	14
	0.50	22	19	20
ZNPs (75°C)	0.25	13	12	11
	0.50	19	17	16
ZnO powder	0.25	6	5	1
	0.50	9	7	3
Control	–	0	0	0
Doxycycline	0.03 mg/disc	30	21	–
Nystatin	0.03 mg/disc	–	–	20

Abbreviations: ZNPs, zinc oxide nanoparticles; ATCC, American Type Culture Collection.

At 75°C, the growth mainly led to the development of a broad arrow-like morphology with fewer slender needle-like formations. The overall growth rate for the broad-arrow ZNP sample at a pH of 11.9 (Figure 3D) is:

$$\mathrm{gr}^{<0\,0\,0\,1>} < \mathrm{gr}^{<0\,1\,\bar{1}\,1>} < \mathrm{gr}^{<0\,1\,\bar{1}\,0>}. \quad [4]$$

These two types of structural growths could be observed in a typical SEM result of 25°C; the majority of these growths were characterized by a typical slender needle-like morphology (in the blue and yellow circle), and few were characterized with broad arrow-like morphologies (in the red circle), as shown in Figure 7.

ZNPs as antimicrobial agents

The effect of metal nanoparticles on pathogenic microbes is an emerging field of research. After successful characterization, the ZNPs synthesized at near-room temperatures were tested for their bactericidal and fungicidal activities. Interestingly, different concentrations of the ZNPs exhibited significant antibacterial activity against both Gram-positive (*S. aureus*) and Gram-negative (*E. coli*) bacteria, as well as activity against a common fungi (*C. albicans*), which is responsible for candidiasis. The concentration-dependent antimicrobial activity expressed in terms of the zone of inhibition was quite visible on NA plates (Figure 8). At the maximum concentrations (0.50 mg/mL), the growth of the microbial strains, namely *S. aureus*, *E. coli*, and *C. albicans*, was reduced significantly (Table 2). At 0.50 mg/mL of the ZNPs, a maximum zone of inhibition (23 mm) was recorded for *S. aureus* by ZNPs synthesized at 55°C. The preliminary data also postulate that the antimicrobial activity of ZNPs may be dependent upon the ZNP's size and morphology. The microbicidal

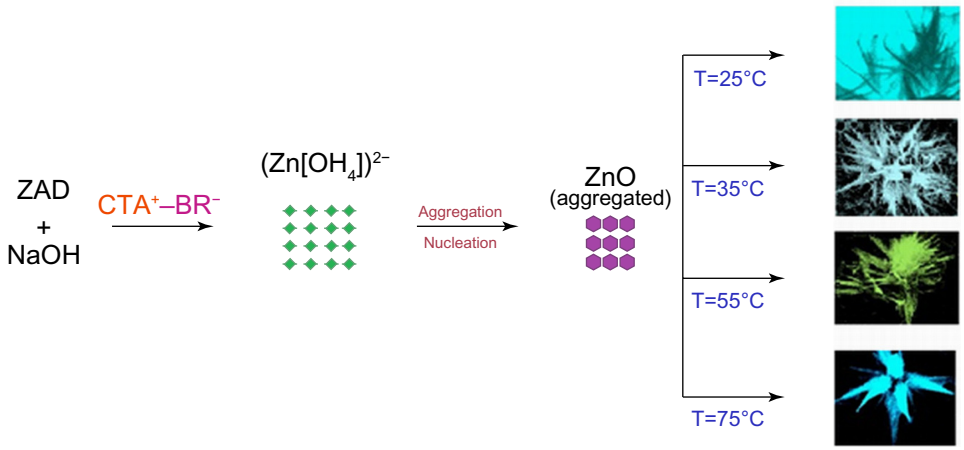

Figure 9 Schematic diagram of the growth mechanism of flower-shaped ZNPs.
Abbreviations: ZAD, zinc acetate dihydrate; CTA, cetyl trimethyl ammonium; T, temperature.

property of these nanoparticles suggested that these particles were more diffusible in the growth medium which, in turn, allowed for a greater interaction between the microbial cells and nanoparticles. Similar microbicidal impacts of some other ZNPs synthesized from different approaches are also known.[53,54] In most of these cases, it has been proposed that these particles interact with thiol groups of vital enzymes and subsequently inactivates them. Even though this might occur, we could not pinpoint the exact site where these ZNPs could affect the microbial cells, but it was very clear that Gram-positive bacterial strains were most susceptible to these ZNPs, which might be due to the presence of special type of cell wall structure that contains different components of charged molecules, such as surface proteins and polysaccharides. Previous reports have indicated that ZNPs' cell surface interactions affect the cell morphology as well as cell membrane's permeability.[55–58] Consequently, the entry of ZNPs induces oxidative stress in the bacterial cells, resulting in the inhibition of cell growth and, eventually, cell death. Overall, the simple mechanism of flower-shaped ZNP growth at near-room temperatures is summarized in Figure 9.

Conclusion

In conclusion, the results showed the synthesis and characterization of flower-shaped ZNPs by a simple sol–gel method at various near-room temperatures (25°C, 35°C, 55°C, and 75°C). The effect of these temperatures on the crystallites' size, pH, and morphology were reported. The SEM results presented the existence of two types of morphologies of flower petals (slender needle-like and broad arrow-like). Therefore, in the ZNP synthesis performed at the lower temperatures, the slender needle-like petals were found in excess as compared to broad arrow-like petals in the various flower bunches of the ZNP colonies. The average crystallite size of the ZNPs was observed as 23.7 nm at 25°C, which is contrary to the size reported at 75°C, which was found to be 88.82 nm. The aspect ratio reached its maximum at lower temperatures, and decreased when moving toward higher temperatures. The sample pH was at its lowest level at 35°C (11.7) and there was a steady increase in sample pH on other temperature ranges. Finally, the growth order of the flower-shaped ZNPs revealed that the growth rate reached its maximum towards (0 0 0 I) and (0 I $\bar{1}$ 0) facets in the growth of slender–slim petals and broad-arrow petals, respectively.

A significant absorbance of light in the UV-B range by the ZNPs clearly demonstrated that ZNPs can be used in sunscreens. In addition, the synthesized ZNPs also showed significant antimicrobial activity, suggesting that ZNPs might be better agents in controlling the spreading of bacterial and fungal infections. A variety of disease-causing bacteria (*S. aureus*) and fungi (*C. albicans*) pose serious threats to contagious skin diseases such as abscesses, furuncles, carbuncles, cellulitis, and candidiasis. Therefore, we can postulate that our synthesized ZNPs, with other formulations, may be externally used as antimicrobial agents in ointments and lotions for the treatment of skin diseases.

Acknowledgments

The authors are thankful to the Department of Science and Technology (DST), Government of India, under the scheme NANOMISSION (Project No SR/NM/NS/91-2008) for their financial support. The authors are also grateful to Dr Ramesh Chandra, Institute Instrumentation Centre, Indian Institute of Technology, Roorkee, India, for his useful suggestions. The authors are also thankful to Mr Wasi and Mr Shamim, University Sophisticated Instruments Facility, Aligarh Muslim University, Aligarh, India, for their efforts in the accomplishment of the SEM results.

Disclosure

The authors report no conflict of interests in this work.

References

1. Zu P, Tang ZK, Wong GKL, et al. Ultraviolet spontaneous and stimulated emissions from ZnO microcrystallite thin films at room temperature. *Solid State Commun*. 1997;103(8):459–463.
2. Kim YS, Tai WP, Shu SJ. Effect of preheating temperature on structural and optical properties of ZnO thin films by sol-gel process. *Thin Solid Films*. 2005;491(1–2):153–160.
3. Becheri A, Dürr M, Lo Nostro P, Baglioni P. Synthesis and characterization of zinc oxide nanoparticles: application to textiles as UV-absorbers. *J Nanopart Res*. 2008;10:679–689.
4. Rao CNR, Müller A, Cheetham AK, editors. *The Chemistry of Nanomaterials: Synthesis, Properties and Applications*. Weinheim, Germany: Wiley-VCH Verlag GmbH & Co. KGaA; 2004.
5. Wu C, Qiao X, Chen J, Wang H, Tan F, Li S. A novel chemical route to prepare ZnO nanoparticles. *Mater Lett*. 2006;60(15):1828–1832.
6. Schmidt-Mende L, MacManus-Driscoll JL. ZnO – nanostructures, defects, and devices. *Mater Today*. 2007;10(5):40–48.
7. Sakohara S, Tickanen LD, Anderson MA. Luminescence properties of thin zinc oxide membranes prepared by the sol-gel technique: change in visible luminescence during firing. *J Phys Chem*. 1992;96(26):11086–11091.
8. Djurišić AB, Ng AMC, Chen XY. ZnO nanostructures for optoelectronics: material properties and device applications. *Progress in Quantum Electronics*. 2010;34(4):191–259.
9. Shrader RE, Leverenz HW. Cathodoluminescence emission spectra of zinc-oxide phosphors. *J Opt Soc Am*. 1947;37(11):939–940.
10. Ashoka S, Chithaiah P, Thipperudraiah KV, Chandrappa GT. Nanostructural zinc oxide hollow spheres: A facile synthesis and catalytic properties. *Inorganica Chimica Acta*. 2010;362(13):3442–3447.
11. Gao PX, Lee JL, Wang ZL. Multicolored ZnO nanowire architectures on trenched silicon substrates. *J Phys Chem C*. 2007;111(37):13763–13769.

12. Liu B, Zeng HC. Hydrothermal synthesis of ZnO nanorods in the diameter regime of 50 nm. *J Am Chem Soc*. 2003;125(15):4430–4431.
13. Li Z, Xiong Y, Xie Y. Selected-control synthesis of ZnO nanowires and nanorods via a PEG-assisted route. *Inorg Chem*. 2003;42(24):8105–8109.
14. Xie J, Li P, Wang Y, Wei Y. Synthesis of needle- and flower-like ZnO microstructures by a simple aqueous solution route. *J Phys Chem Solids*. 2009;70(1):112–116.
15. Wei A, Sun XW, Xu CX, et al. Growth mechanism of tubular ZnO formed in aqueous solution. *Nanotechnology*. 2006;17(6):1740–1744.
16. Gui Z, Liu J, Wang Z, et al. From multicomponent precursor to nanoparticle nanoribbons of ZnO. *J Phys Chem B*. 2005;109(3):1113–1117.
17. Ni YH, Wei XW, Ma X, Hong JM. CTAB assisted one-pot hydrothermal synthesis of columnar hexagonal-shaped ZnO crystals. *J Cryst Growth*. 2005;283(1–2):48–56.
18. Zhao H, Su X, Xiao F, Wang J, Jian J. Synthesis and gas sensor properties of flower-like 3D ZnO microstructures. *Materials Science and Engineering: B*. 2011;176(7):611–615.
19. Bahnemann DW, Kormann C, Hoffmann MR. Preparation and characterization of quantum size zinc oxide: a detailed spectroscopic study. *J Phys Chem*. 1987;91(14):3789–3798.
20. Spanhel L, Anderson MA. Semiconductor clusters in the sol-gel process: quantized aggregation, gelation, and crystal growth in concentrated zinc oxide colloids. *J Am Chem Soc*. 1991;113(8):2826–2833.
21. Tokumoto MS, Pulcinelli SH, Santilli CV, Briois V. Catalysis and temperature dependence on the formation of ZnO nanoparticles and zinc acetate derivatives prepared by the sol-gel route. *J Phys Chem B*. 2003;107(2):568–574.
22. Meulenkamp EA. Synthesis and growth of ZnO nanoparticles. *J Phys Chem B*. 1998;102(29):5566–5572.
23. Sivakumar R, Tsunoda T, Kuroki Y, Okamoto T, Takata M. ZnO nanowire growth by electric current heating method: a study on the effect of substrate temperature. *Mater Chem Phys*. 2012;134(1):345–349.
24. Bilecka I, Elser P, Niederberger M. Kinetic and thermodynamic aspects in the microwave-assisted synthesis of ZnO nanoparticles in benzyl alcohol. *ACS Nano*. 2009;3(2):467–477.
25. Chen Y, Yu R, Shi Q, Qin J, Zheng F. Hydrothermal synthesis of hexagonal ZnO clusters. *Mater Lett*. 2007;61(22):4438–4441.
26. Hwang CC, Lin CS, Wang GP, Peng CH, Chung SL. A self-propagating high-temperature synthesis method for synthesis of zinc oxide powder. *J Alloys Compd*. 2009;467(1–2):514–523.
27. Yu Q, Fu W, Yu C, et al. Fabrication and optical properties of large-scale ZnO nanotube bundles via a simple solution route. *J Phys Chem C*. 2007;111(47):17521–17526.
28. Zhao W, Song X, Yin Z, Fan C, Chen G, Sun S. Self-assembly of ZnO nanosheets into nanoflowers at room temperature. *Mater Res Bull*. 2008;43(11):3171–3176.
29. Haile SM, Johnson DW Jr, Wiseman GH, Bowen HK. Aqueous precipitation of spherical zinc oxide powders for varistor applications. *J Am Ceram Soc*. 1989;72(10):2004–2008.
30. Zhang S, Yao S, Li J, Zhao L, Wang J, Boughton RI. Growth habit control of ZnO single crystals in molten hydrous alkali solutions. *J Cryst Growth*. 2011;336(1):56–59.
31. Umar A, Kim SH, Suh EK, Hahn YB. Ultraviolet-emitting javelin-like ZnO nanorods by thermal evaporation: growth mechanism, structural and optical properties. *Chem Phys Lett*. 2007;440(1–3):110–115.
32. Zhang H, Yang D, Ji Y, Ma X, Xu J, Que D. Low temperature synthesis of flowerlike ZnO nanostructures by cetyltrimethylammonium bromide-assisted hydrothermal process. *J Phys Chem B*. 2004;108(13):3955–3958.
33. Yin H, Xu Z, Wang Q, Bai J, Bao H. Study of assembling ZnO nanorods into chrysanthemum-like crystals. *Mater Chem Phys*. 2005;91(1):130–133.
34. Ni Y, Wu G, Zhang X, et al. Hydrothermal preparation, characterization and property research of flowerlike ZnO nanocrystals built up by nanoflakes. *Mater Res Bull*. 2008;43(11):2919–2928.
35. Li F, Hu L, Li Z, Huang X. Influence of temperature on the morphology and luminescence of ZnO micro and nanostructures prepared by CTAB-assisted hydrothermal method. *J Alloys Compd*. 2008;465(1–2):L14–L19.
36. Li H, Ni Y, Hong J. Ultrasound-assisted preparation, characterization and properties of flower-like ZnO microstructures. *Scr Mater*. 2009;60(7):524–527.
37. Khan MF, Hameedullah M, Ansari AH, inventors Aligarh Muslim University, assignee. Production of nanoscale zinc oxide colloidal solution for pharmaceutical and scientific applications. India patent 1583/DE/2011 A.
38. Chen HC, Hua MY, Liu YC, Yang HW, Tsai RY. Preparation of water-dispersible poly[aniline-co-sodium N-(1-one-butyric acid) aniline]-zinc oxide nanocomposite for utilization in an electrochemical sensor. *J Mater Chem*. 2012;22:13252–13259.
39. Cullity BD. *Elements of X Ray Diffraction*. Reading, MA: Addison-Wesley Publishing Company; 1956.
40. Erol A, Okur S, Comba B, Mermer Ö, Arikan MÇ. Humidity sensing properties of ZnO nanoparticles synthesized by sol-gel process. *Sens Actuators B Chem*. 2010;145(1):174–180.
41. Jain N, Bhargava A, Tarafdar JC, Singh SK, Panwar J. A biomimetic approach towards synthesis of zinc oxide nanoparticles. *Appl Microbiol Biotechnol*. 2013;97(2):859–869.
42. Zak AK, Razali R, Majid WH, Darroudi M. Synthesis and characterization of a narrow size distribution of zinc oxide nanoparticles. *Int J Nanomedicine*. 2011;6:1399–1403.
43. Bauer AW, Kirby WM, Sherris JC, Turck M. Antibiotic susceptibility testing by a standardized single disk method. *Am J Clin Pathol*. 1966;45(4):493–496.
44. Musthafa TNM, Siddiqui ZN, Husain FM, Ahmad I. Microwave-assisted solvent-free synthesis of biologically active novel heterocycles from 3-formylchromones. *Med Chem Res*. 2011;20(9):1473–1481.
45. Rekha K, Nirmala M, Nair MG, Anukaliani A. Structural, optical, photocatalytic and antibacterial activity of zinc oxide and manganese doped zinc oxide nanoparticles. *Physica B Condens Matter*. 2010;405(15):3180–3185.
46. Lin HF, Liao SC, Hung SW. The dc thermal plasma synthesis of ZnO nanoparticles for visible-light photocatalyst. *J Photochem Photobiol A Chem*. 2005;174(1):82–87.
47. Guan XH, Wang GS, Li CP, Lv YZ, Guo L, Xu HB. Synthesis and optical properties of ZnO multipod nanorods. *J Lumin*. 2007;122–123:770–772.
48. Hale PS, Maddox LM, Shapter JG, Voelcker NH, Ford MJ, Waclawik ER. Growth kinetics and modeling of ZnO nanoparticles. *J Chem Educ*. 2005;82(5):775–778.
49. Zhang H, Yang D, Ma X, Ji Y, Xu J, Que D. Synthesis of flower-like ZnO nanostructures by an organic-free hydrothermal process. *Nanotechnology*. 2004;15(5):622–626.
50. Bahadur H, Srivastava AK, Sharma RK, Chandra S. Morphologies of sol–gel derived thin films of ZnO using different precursor materials and their nanostructures. *Nanoscale Res Lett*. 2007;2(10):469–475.
51. Ahsanulhaq Q, Kim SH, Kim JH, Hahn YB. Structural properties and growth mechanism of flower-like ZnO structures obtained by simple solution method. *Mater Res Bull*. 2008;43(12):3483–3489.
52. Rai P, Jo JN, Lee IH, Yu YT. Fabrication of flower-like ZnO microstructures from ZnO nanorods and their photoluminescence properties. *Mater Chem Phys*. 2010;124(1):406–412.
53. Wahab R, Kim YS, Mishra A, Yun SI, Shin HS. Formation of ZnO micro-flowers prepared via solution process and their antibacterial activity. *Nanoscale Res Lett*. 2010;5(10):1675–1681.
54. Wang C, Liu LL, Zhang AT, Xie P, Lu JJ, Zou XT. Antibacterial effects of zinc oxide nanoparticles on Escherichia coli. *African Journal of Biotechnology*. 2012;11(44):10248–10254.
55. He L, Liu Y, Mustapha A, Lin M. Antifungal activity of zinc oxide nanoparticles against Botrytis cinerea and Penicillium expansum. *Microbiol Res*. 2011;166(3):207–215.

56. Jiang W, Mashayekhi H, Xing B. Bacterial toxicity comparison between nano- and micro-scaled oxide particles. *Environ Pollut*. 2009;157(5):1619–1625.
57. Jin T, Sun D, Su Y, Zhang H, Sue HJ. Antimicrobial efficacy of zinc oxide quantum dots against Listeria monocytogenes, Salmonella Enteritidis and Escherichia coli O157:H7. *J Food Sci*. 2009;74(1):M46–52.
58. Xie Y, He Y, Irwin PL, Jin T, Shi X. Antibacterial activity and mechanism of action of zinc oxide nanoparticles against Campylobacter jejuni. *Appl Environ Microbiol*. 2011;77(7):2325–2331.